creative commons
COMMONS DEED

저작자표시-비영리-변경금지 2.0 대한민국

이용자는 아래의 조건을 따르는 경우에 한하여 자유롭게

- 이 저작물을 복제, 배포, 전송, 전시, 공연 및 방송할 수 있습니다.

다음과 같은 조건을 따라야 합니다:

저작자표시. 귀하는 원저작자를 표시하여야 합니다.

비영리. 귀하는 이 저작물을 영리 목적으로 이용할 수 없습니다.

변경금지. 귀하는 이 저작물을 개작, 변형 또는 가공할 수 없습니다.

- 귀하는, 이 저작물의 재이용이나 배포의 경우, 이 저작물에 적용된 이용허락조건을 명확하게 나타내어야 합니다.
- 저작권자로부터 별도의 허가를 받으면 이러한 조건들은 적용되지 않습니다.

저작권법에 따른 이용자의 권리는 위의 내용에 의하여 영향을 받지 않습니다.

이것은 이용허락규약(Legal Code)을 이해하기 쉽게 요약한 것입니다.

Disclaimer

dCollection

연세대학교
YONSEI UNIVERSITY

Evaluation the molecular pathophysiological characteristics of sinonasal undifferentiated carcinoma (SNUC)

Hyang Joo Ryu

Department of Medicine

The Graduate School, Yonsei University

연세대학교
YONSEI UNIVERSITY

Evaluation the molecular pathophysiological characteristics of sinonasal undifferentiated carcinoma (SNUC)

Directed by Professor Sun Och Yoon

The Doctoral Dissertation
submitted to the Department of Medicine,
the Graduate School of Yonsei University
in partial fulfillment of the requirements for the degree of
Doctor of Philosophy in Medical Science

Hyang Joo Ryu

December 2023

연세대학교
YONSEI UNIVERSITY

This certifies that the Doctoral Dissertation of
Hyang Joo Ryu is approved.

Thesis Supervisor: Sun Och Yoon

Thesis Committee Member#1: Se-Hoon Kim

Thesis Committee Member#2: Hye Ryun Kim

Thesis Committee Member#3: Joon Seon Song

Thesis Committee Member#4: Sangwoo Kim

The Graduate School
Yonsei University

December 2023

연세대학교
YONSEI UNIVERSITY

ACKNOWLEDGEMENTS

I would like to express my gratitude to Professor Sun Och Yoon, who is my supervisor. I am truly grateful to Professors Se-Hoon Kim, Hye Ryun Kim, Joon Seon Song, and Sangwoo Kim for their invaluable guidance, which led this research in the right direction. Thank you to my husband, JaeHyeong Jung, my son, Sun-Yul Jung, and my mom and dad who have always been by my side and have given me constant support and love. Lastly, I am grateful to my sincere colleague, Milim Kim, who gave me strength and courage during this long journey.

연세대학교
YONSEI UNIVERSITY

<TABLE OF CONTENTS>

연세대학교
YONSEI UNIVERSITY

연세대학교
YONSEI UNIVERSITY

LIST OF FIGURES

연세대학교
YONSEI UNIVERSITY

연세대학교
YONSEI UNIVERSITY

LIST OF TABLES

연세대학교
YONSEI UNIVERSITY

ABSTRACT

Evaluation the molecular pathophysiological characteristics of sinonasal undifferentiated carcinoma (SNUC)

Hyang Joo Ryu

Department of Medicine
The Graduate School, Yonsei University

(Directed by Professor Sun Och Yoon)

Sinonasal undifferentiated carcinoma (SNUC) is a rare and highly aggressive malignancy originating in the nasal cavity and paranasal sinuses. Diagnosis is challenging, primarily relying on excluding differentiation into squamous, glandular, or neuroendocrine cells. SNUC exhibits a poor prognosis, with a limited understanding of its pathogenesis and immune characteristics.

In this study, we explored SNUC's molecular features, focusing on tumorigenesis and immunity. Spatial transcriptome analysis revealed activated chromatin remodeling and histone modification pathways as well as *EZH2* gene upregulation, suggesting epigenetic mechanisms may involved in SNUC carcinogenesis. Genetic mutations associated with these pathways were not prevalent, suggesting alternative regulatory mechanisms.

In vitro analyses, mRNA and protein of EZH2 with other polycomb repressive complex 2 (PRC2)-related chromatin remodeling markers such as SUZ12 and EED were more upregulated while squamous cell differentiation markers such as p40, p63, KRT5, and KRT6 were more decreased in undifferentiated carcinoma than differentiated squamous cell carcinoma of head and neck. Clinical tissues of SNUC validated these results by showing increased immunoexpression of EZH2 and other PRC2 markers. The present findings suggest a pivotal role for EZH2 in driving undifferentiated carcinoma progression. In the present study, no specific findings were identified for the role of tumor immunity in SNUC development.

연세대학교
YONSEI UNIVERSITY

Epigenetic modifications, induced by EZH2 activation are likely key drivers of SNUC pathogenesis. EZH2, identified as a potential therapeutic target, demonstrates its oncogenic significance across various cancer types, including SNUC. Despite the relatively immune-poor microenvironment observed in SNUC, further investigation is needed to discern its role in SNUC development and potential immune escape mechanisms. In summary, our study sheds light on the molecular underpinnings of SNUC, emphasizing epigenetic regulation and EZH2 as a promising therapeutic target for this aggressive malignancy.

Keywords: EZH2, Sinonasal undifferentiated carcinoma, polycomb repressive complex, undifferentiated

연세대학교
YONSEI UNIVERSITY

Evaluation the molecular pathophysiological characteristics of sinonasal undifferentiated carcinoma (SNUC)

Hyang Joo Ryu

Department of Medicine
The Graduate School, Yonsei University

(Directed by Professor Sun Och Yoon)

I. INTRODUCTION

Sinonasal undifferentiated carcinoma (SNUC) is a malignant epithelial tumor that originates in the nasal cavity and paranasal sinuses. The diagnosis of SNUC is established when cytokeratin-positive tumor cells exhibit no histological or immunohistochemical evidence of differentiation into squamous, glandular, or neuroendocrine cells. Therefore, SNUC is typically a diagnosis made by excluding other possibilities [1]. SNUC is rare and occupies about 3-5% of sinonasal carcinomas. This tumor is typically referred to as a highly aggressive cancer, showing a poor prognosis, with approximately a 35% of 5-year survival rate. Upon diagnosis, SNUC often presents with very large-sized, rapidly growing masses, involving multiple sites within the sinonasal tract, and invading surrounding structures such as the orbital cavity, skull base, and brain.[1-3]. SNUC was first described in 1986 [3], however, the pathogenesis of this tumor remains limited.

Studies on the carcinogenesis of SNUC have indicated a relationship between tumor development and recurrent *IDH2* R172 mutation [4-6], which mutation induced H3 lysin methylation and DNA hypermethylation [7], alterations in the SWI/SNF chromatin

연세대학교
YONSEI UNIVERSITY

remodeling complex [8], which roles in tumor suppression [9], and *PGAP3-SRPK1* fusion [8], which remains unknown but plays an oncogenic role in SNUC have been identified. However, these limited results do not suggest the pathogenesis of tumor development in SNUC.

Regarding the tumor immunity of SNUC, a case report documented a complete response following anti-PD-1 immunotherapy in one SNUC patient [10], however, its aspect on immunity in SNUC remains insufficient [10, 11].

Although the tumor immune microenvironment (TIME) concept recently emerged regarding in tumor development [12, 13], studies about tumor immunity of SNUC are limited and the role of TIME is not well elucidated in SNUC.

Probably due to the rare incidence and lack of understanding of the pathophysiology of SNUC, there has been no standardized treatment regimen for this aggressive tumor [14, 15].

Limited research on SNUC may be attributed to technical challenges including difficulties in accessing the lesion site, obtaining only small-sized tissue samples owing to rapid tumor growth, or occasionally subjection the samples to a decalcification process. These challenges make it difficult to obtain an adequate number of viable SNUC tumor cells, hindering the establishment of cell lines of animal models for experiments.

In this study, we focused on the carcinogenesis and tumor immunity of SNUC to address the technical problems. First, spatial analysis of the tumor transcriptome in situ within the SNUC tissue was performed. Second, we compared the gene expression profiles of tumor cells with those of normal epithelial cells in the sinonasal tract to elucidate the carcinogenesis of SNUC. Third, we compared the transcript levels of tumor-infiltrating immune cells with those of immune cells in tumor-free normal tissue areas to investigate the potential role of the tumor immune microenvironment (TIME) in SNUC. Finally, our results were validated using clinical tissue samples and in vitro cell lines. Overall, this study aimed to identify the molecular characteristics that may play crucial roles in the development of SNUC, particularly in terms of carcinogenesis and tumor immunity.

연세대학교
YONSEI UNIVERSITY

II. MATERIALS AND METHODS

1. Patients, samples, and clinical data

From the database of Severance Hospital Cancer Registry Data, Seoul, Korea, about 30 cases that underwent surgically excised or biopsied tissue were retrieved; these cases were diagnosed as primary sinonasal undifferentiated carcinoma at Severance Hospital. All cases were pathologically diagnosed as sinonasal undifferentiated carcinoma at Severance Hospital. Archived formalin-fixed, paraffin-embedded (FFPE) samples were obtained. However, samples that had undergone decalcification or chemotherapy or had a limited number of tumor cells were excluded. Finally, 23 cases were obtained. To select the most representative sections, samples were mounted on the slides, stained with haematoxylin and eosin (H&E), and reviewed by two pathologists (H.J.R & S.O.Y). We obtained the tumor samples of patients. All methods and experimental protocols using human tissues were carried out in accordance with relevant guidelines and regulations approved by the Institutional Review Board of Severance Hospital, Yonsei University Health System (IRB no. 4-2022-0466).

2. Immunohistochemical staining, in situ hybridization and microscopic analysis

The representative slides were selected for immunohistochemistry. Immunohistochemistry was performed on 4-μm TMA sections with a Ventana BenchMark XT Autostainer (Ventana Medical Systems, Tucson, AZ, USA), according to the manufacturer's instructions. Primary antibodies were CK(AE1/AE3) (1:50, clones AE1/AE3; Dako), p40 (RTU, polyclonal; Biocare), p63 (1:50, clone DAK-p63; Dako), CK5/6 (1:50, clone D5/16 B4; Dako), p16 (RTU; Ventana), CK7 (1:100, clone OV-TL 12-30; Dako), NUT (1:50, clone C52B1; Cell signaling), Synaptophysin (1:50, clone DAK-SYNAP; Dako),

연세대학교
YONSEI UNIVERSITY

Chromogranin A (1:100, clone DAK-A3; Dako), INI-1(SMARCB1) (1:200, clone BAF47; BD), BRG1(SMARCA4) (1:200, clone EPNCIR111A; Abcam), EZH2 (1:20, clone ZMD.309; Invitrogen, Carlsbad, CA, USA), BMI1 (1:100, clone clone 1.T.21; Abcam), SUZ12 (1:50, clone SUZ220A; Abcam, Cambridge, MA, USA), EED (1:100, clone 163C; Abcam) and H3K27me3 (1:200, clone C36B11; Abcam). In situ hybridization (ISH) has been performed using the *Ventana EBER ISH iView Blue Plus Kit*. Semi-quantitative or qualitative analyses of each marker were microscopically performed by expert pathologists according to the criteria of cutoff-value (generally, more than 10% for positive expression) or H-score (on a scale of 0-300).

3. Multiplex digital spatial profiling (DSP) analysis

The NanoString GeoMx DSP assay (NanoString Technologies, Seattle, WA, USA) was performed in 23 cases of SNUC. Briefly, one to two tumor cores from representative sections with one normal core were extracted from formalin-fixed paraffin-embedded (FFPE) tissue blocks in each case using a 2-mm sized punch, and they were made into a tissue microarray (TMA). A total of 38 TMA cores, which contain 27 cores of the tumor area and 11 cores of the normal area. As a result, 11 cases among 23 cases were paired. Pan-cytokeratin, CD45, and Smooth muscle actin (SMA) were stained using an immunofluorescence assay for differential visualization of three primary cell types (carcinoma cells, lymphocytes, and stromal fibroblastic cells, respectively) on the TMA slide. One to three geometric regions of interest (ROI) were targeted in every TMA core (Total ROIs, n=48; Tumor ROIs, n=37; Normal ROIs, n=11). We used a validated panel, GeoMx Whole Transcriptome Atlas (Human RNA) with NGS readout (NanoString Technologies), which contains more than 1800 RNA targets. The selection of each ROI was performed by expert pathologists. All ROIs underwent QC testing using the Q3 normalization method, and they all passed the QC test.

연세대학교
YONSEI UNIVERSITY

4. Next-generation sequencing(NGS) analysis

Targeted deep sequencing analyses, including related experiments and genome analyses, were performed at Macrogen (Seoul, Korea), using FFPE DNA from SNUC tissue samples. FFPE DNA was extracted using the QIAamp DNA FFPE Tissue Kit (Qiagen, Valencia, CA, USA) following the manufacturer's instructions. Initial quality checks were performed using electrophoresis on 1% agarose gels and the Qubit dsDNA HS Assay Kit (Life Technologies, Carlsbad, CA, USA). The FFPE DNA was then sheared into fragments of mean peak size 180200 bp using Adaptive Focused Acoustics (Covaris, Woburn, MA, USA). Libraries were prepared using the SureSelect XT protocol (Agilent Technologies, Santa Clara, CA, USA) with the Axen™ Cancer Master panel (Macrogen, Seoul, Korea). Library quality was checked with the 2100 Bioanalyzer (Agilent), requiring a product size of 200-400 bp. The libraries were sequenced paired-end (2 x 150 bp) on a NextSeq500 instrument to approximately 2,000X coverage. Adapter sequences were removed, and reads were aligned to the reference genome (GRCh37/hg19) using BWA-MEM [16]. Poorly mapped reads with MAPQ below 20 were removed. Duplicated reads were discarded, and base quality was recalibrated. Somatic mutations, including single nucleotide variants (SNVs) and small insertions and deletions (INDELs), were identified using the MuTect2 algorithm [17]. False positive variant calls from oxo artifacts were excluded, as well as mutations below 2% VAF and 100X total depth. Germline variants were excluded based on MAF in ExAC_EAS or Macrogen Korean Population Database. The remaining variants were annotated using SnpEff & SnpSift v4.3i with dbNSFP v2.9.3. MSI was calculated using mSINGS, and TMB was reported as the number of mutations per megabase of passed missense mutations.

5. In vitro analysis

연세대학교
YONSEI UNIVERSITY

Human head and neck squamous cell carcinoma cell lines, SNU1066, SNU1076, and YD10B were purchased from Korean Cell Line Bank (Seoul, South Korea). FaDu (ATCC® HTB-43™, pharynx SCC) and human anaplastic squamous cell carcinoma cell line, CCL 30 (RPMI 2650) were purchased from American Type Culture Collection (ATCC). SNU1066, SNU1076, and YD-10B were cultivated in DMEM media (11995-065, Gibco, USA) supplemented with 10% fetal bovine serum, 1% penicillin, and streptomycin at 37 ℃ in a humidified incubator with 5% CO2. FaDu and CCL30 were cultivated in Minimun Essential Medium (MEM) (11095-080, Gibco, USA) media supplemented with 10% fetal bovine serum, 1% penicillin, and streptomycin at 37 ℃ in a humidified incubator with 5% CO2. DMEM and MEM medium, fetal bovine serum, phosphate-buffered saline (PBS), and penicillin-streptomycin were obtained from Gibco, USA.

A. Quantitative reverse transcription polymerase chain reaction (qRT-PCR)

RNA was isolated using RNeasy Plus Mini Kits (74134, Qiagen, Carlsbad, CA, USA), and cDNA was synthesized using SensiFAST cDNA Synthesis Kit (BIO-65054, Meridian Bioscience, Memphis, TN, USA). Primers for p40, p63, cytokeratin5, cytokeratin6, and GAPDH were manufactured (BIONEER, Daejeon, Korea). Using SensiFAST SYBR Lo-Rox Kit (BIO-94020, Meridian Bioscience) as PCR reagent and the Applied Biosystems™ QuantStudio™ 3 Real-Time PCR System (Thermo Scientific, Logan, UT, USA), PCR was performed at 95 °C for 2 min; at 95 °C for 5 s and 58 °C for 20 s over 45 cycles; 95 °C for 15 s; 60 °C for 1 min; and 95 °C for 15 s. Experiments were performed independently three or more times. The primer sequences for qRT-PCR are given in Table 1.

연세대학교
YONSEI UNIVERSITY

Table 1. The primer sequences for qRT-PCR.

Gene name	Forward	Reverse
EZH2	TCGAGCTCCTCTG AAGCAAA	AGTATCCACATC CTCAGCGG
SUZ12	CTCTGAACTGCCG CAAACTT	CTCTTAACTGGT CCGTTGCG
EED1	TGCGATGGTTAGG CGATTTG	CCAAATGTCACA CTGGCTGT
BMI1	TTGTTTGCCTAGC CCCAGTA	GAAGAAGTTGCT GATGACCCA
P40	GCCACAGTACACG AACCTGG	GCACGTGGTCTG TGTTATAGGGAC
P63	GAAAGAAAGTTAT TACCGATCCAC	CTGTT CCAGAAAATCCC AG
Cytokeratin 5	CAAGGTTGATGCA CTGATGG	TCAGCGATGATG CTATCCAG
Cytokeratin 6	GACCTGGTGGAGG ACTTCAA	GTAGGCAGCATC CACATCCT
GAPDH	ACCCAGAAGACTG TGGATGG	CACATTGGGGGT AGGAACAC

B. Western blotting

FaDu, SNU1066, SNU1076, YD10B, and CCL30 were seeded onto 100 mm dishes then cultured in MEM media for FaDu and CCL30, in DMEM media for SUN1076, SNU1066, YD-10B. Protein extracts were obtained from cell lines, using a protein extract solution (RIPA Lysis and Extraction Buffer; Thermo Scientific™, USA) following the manufacturer's instructions. Proteins from

연세대학교
YONSEI UNIVERSITY

lysates were loaded on Q-PAGE™ TGN Precast Gel (QP4520, SMOBIO Technology, Paramount, CA, USA). Gels were transferred to PVDF Membrane (IPVH00010, Merck Millipore, Middlesex, MA, USA). Antibodies used for Western blot analysis included anti-EZH2 (Invitrogen, USA), anti-SUZ12 (Abcam, USA), anti-EED (Abcam, USA), anti-BMI1 (Abcam, USA), anti-p63 (Dako, Denmark), anti-cytokeratin5/6 (Dako, Denmark) and β-actin (Invitrogen, USA).

C. Morphologic evaluation of cell lines.

Microscopic features of the five cell lines of FaDu, SNU1066, SNU1076, YD10B, and CCL30. Cells were captured at 20x magnification of the culture dish under the light microscope (BX43, Olympus). To observe the details under the light microscopic examination, cells were detached using trypsin-EDTA, washed with PBS, spin-down in the high-speed centrifuge, undergone in the process of liquid-based cytology preparation, and stained with Papani-colau (PAP) method on liquid-based cytology preparation (LBP) slides.

6. Estimated immune and stromal cell profile using SpatialDecon library with SafeTME matrix

To identify immune cell and stromal cell profiles within SNUC samples, SpatialDecon analysis was performed using SafeTME cell profile matrix from 75th percentile normalized RNA expression data. The matrix of estimated immune cell types of each ROI was depicted in heatmap. The detailed method is described in previous research [18].

7. Statistical analysis

Chi-square, Fisher’s exact test, Student's t-test, and Wilcoxon-signed rank test were used to evaluate the statistical significance between the two variables. P values less than 0.05 were considered significant with all reported p values being

연세대학교
YONSEI UNIVERSITY

two-sided. All data were analyzed using R software (version 4.3.1). Three independent Western Blots were quantified using Image J Software. The protein expression was normalized with respect to the corresponding Beta-actin signals of the appropriate samples.

연세대학교
YONSEI UNIVERSITY

III. RESULTS

1. Clinical and pathological features

The clinical characteristics of the samples are summarized in Table 2. The cohort consisted of 17 (74%) men and six (26%) women, the median patient age was 54 years. More than half (13/23, 57%) of cases were diagnosed at the advanced tumor stage of AJCC III-IV. The median disease-specific survival period was 60.4 months. Among 23 patients, distant metastasis was observed in 6 (26%) patients.

Table 2. Clinical characteristics of 23 patients with Sinonasal undifferentiated carcinoma (SNUC)

Characteristics	Number (%)
Age, median (range), years	54 (29-86)
Sex	
Male	17 (73.9)
Female	6 (26.1)
Initial stage, according to AJCC stage	
I	1 (4.3)
IIB	1 (4.3)
III	3 (13.1)
IV	10 (43.5)
Unknown	8 (34.8)
Metastasis	
Absent	17 (73.9)

연세대학교
YONSEI UNIVERSITY

Present	6 (26.1)
Liver	1
Bone	3
Lung	1
Distant lymph node	1
Overall disease-specific survival, median	60.4 months

2. Histologic, immunohistochemical, and in situ hybridization features

The histologic diagnosis followed the definition of SNUC of WHO tumor classification 5th edition [1]; SNUC shows no specific differentiation into squamous, glandular, or neuroendocrine lineage in histology and immunophenotype.

Histologically, tumor cells reveal large-sized, monotonous, undifferentiated cell morphology with large nucleoli and scant cytoplasm in the overall of included 23 cases. Squamous or glandular differentiation was not identified. In most cases (91.3%, 21/23 cases) variable extent of tumor necrosis is accompanied.

The results of immunohistochemistry studies are summarized in Table 3. All cases revealed cytokeratin expression with variable intensity and proportion. Other tested markers did not show significant positivity for squamous differentiation (p40, p63), glandular differentiation (CK7), neuroendocrine differentiation (synaptophysin, chromogranin), NUT expression, Human papillomavirus (HPV) association (p16), Epstein-Barr virus (EBV) infection (EBER) or deficiency of INI1 (SMARCB1) and BRG1 (SMARCA4). Only one case revealed loss of BRG1 (SMARCA4). However, in this case, Next Generation Sequencing (NGS) analysis revealed no genetic mutation of

연세대학교
YONSEI UNIVERSITY

SMARCA4, and it was included in the study. The representative images are described in Figure 1.

Table 3. Results of immunohistochemistry (IHC) and in situ hybridization (ISH)

IHC and ISH	Cut off value for positivity	Positive results, n (%)
Cytokeratin	>5%, if any	23, 100%
p40	>10%	5, 21.7%
p63	>10%	5, 21.7%
CK7	>10%	0, 0%
Synaptophysin	>10%	0, 0%
ChromograninA	>10%	0, 0%
p16	>70%	1, 4.3%
NUT	0	0, 0%
INI1 (SMARCB1)	Complete loss	0, 0%
BRG1 (SMARCA4)	Complete loss	1, 4.3%
EBER	>10%	9, 39.1%

Abbreviation: IHC, immunohistochemistry; ISH, in situ hybridization; EBER, Epstein-Barr virus (EBV)-encoded small RNAs

연세대학교
YONSEI UNIVERSITY

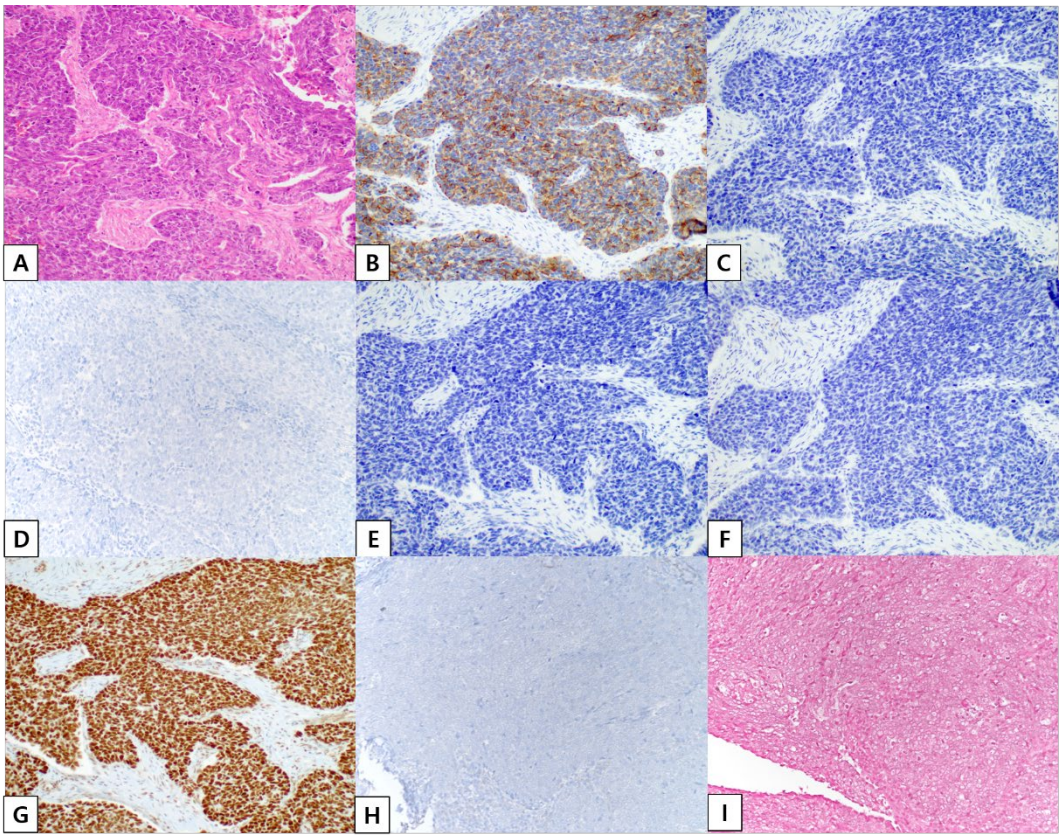

Figure 1. Representative images of Sinonasal undifferentiated carcinoma (SNUC) in HE stain slide image (A), immunohistochemical staining, and in situ hybridization images. Diffuse infiltration of undifferentiated carcinoma cells with numerous mitotic features without specific growth patterns. The tumor cells are focally positive in CK(AE1/AE3) (B), p40 negative (C), CK7 negative (D), and negative for Synaptophysin (E) and chromogranin A (F). All cases were retained expression for INI1 (G). All cases were negative for NUT (H) and most of the cases were negative for EBER in situ hybridization (I).

3. Spatial transcriptome analysis

A. Spatial transcriptome features regarding carcinogenesis

연세대학교
YONSEI UNIVERSITY

For GeoMx™ multiplex DSP analysis, 48 ROIs were selected. These ROIs were collected from the tumor tissue areas (37 ROIs) and normal tissue areas (11 ROIs) (Figure 2). To segment the epithelial cells, including tumor cells and normal epithelial cells, cytokeratin (CK) positive signals were evaluated and compared with H&E-stained microscopic morphology. As a result, a total of 36 ROIs were selected with 28 ROIs of the tumor epithelial cell area and 8 ROIs of normal epithelium area. For segmentation of immune cells, CD45 positive signals were evaluated with H&E- stained microscopic morphology, and a total of 10 ROIs were selected with 7 ROIs of the tumor-infiltrating immune cell area and 3 ROIs of the normal area. Details are summarized in Figure 3.

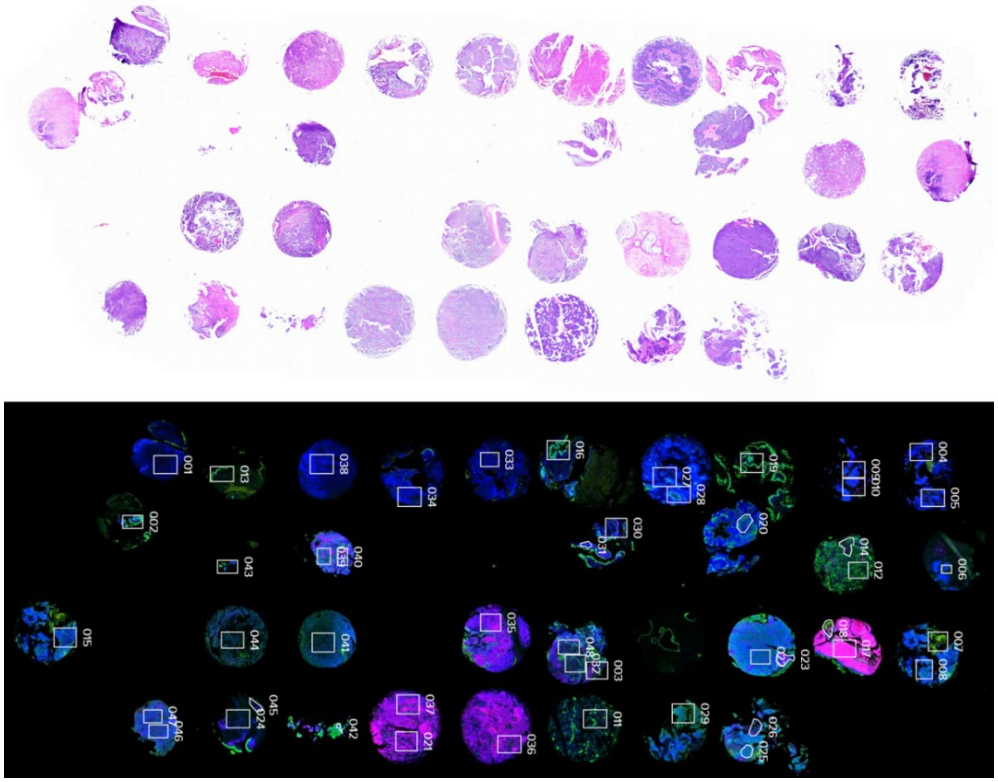

Figure 2. Representative H&E slide image and immunofluorescence images for DSP analysis.

연세대학교
YONSEI UNIVERSITY

ID	TN	Prognosis	Metastasis	ROILabel	SegmentLabel
SNUC_01	Tumor	Poor	NonMeta	1	CK+
SNUC_02	Normal	Good	NonMeta	13	CK+
	Normal	Good	NonMeta	16	CK+
	Tumor	Good	NonMeta	33	CK+
	Tumor	Good	NonMeta	34	CK+
SNUC_03	Tumor	Good	NonMeta	38	CK+
	Normal	Good	NonMeta	19	CK+
	Tumor	Good	NonMeta	27	CK+
	Tumor	Good	NonMeta	28	CK+
SNUC_04	Tumor	Good	NonMeta	9	CK+
	Tumor	Good	NonMeta	10	CD45+
SNUC_05	Normal	Good	NonMeta	2	CK+
	Tumor	Good	NonMeta	4	CK+
	Tumor	Good	NonMeta	5	CK+
SNUC_06	Tumor	Poor	NonMeta	43	CK+
SNUC_07	Tumor	Good	NonMeta	39	CK+
	Tumor	Good	NonMeta	40	CD45+
SNUC_10	Tumor	Poor	Meta	30	CK+
	Tumor	Poor	Meta	31	CK+
SNUC_11	Normal	Good	NonMeta	12	CK+
	Normal	Good	NonMeta	14	CD45+
	Tumor	Good	NonMeta	20	CK+
SNUC_12	Tumor	Good	NonMeta	6	CK+
	Normal	Good	NonMeta	15	CK+
SNUC_13	Tumor	Poor	NonMeta	41	CK+
	Tumor	Poor	NonMeta	44	CK+

ID	TN	Prognosis	Metastasis	ROILabel	SegmentLabel
SNUC_14	Normal	Good	NonMeta	35	CD45+
SNUC_15	Tumor	Good	NonMeta	3	CD45+
	Tumor	Good	NonMeta	32	CK+
	Tumor	Good	NonMeta	48	SMA+
SNUC_16	Normal	Good	NonMeta	17	CD45+
	Normal	Good	NonMeta	18	CK+
	Tumor	Good	NonMeta	22	CK+
	Tumor	Good	NonMeta	23	CD45+
SNUC_17	Tumor	Good	NonMeta	7	CK+
	Tumor	Good	NonMeta	8	CK+
SNUC_18	Tumor	Good	NonMeta	46	CK+
	Tumor	Good	NonMeta	47	CD45+
SNUC_19	Tumor	Poor	Meta	24	SMA+
	Tumor	Poor	Meta	45	CK+
SNUC_20	Tumor	Poor	Meta	42	CK+
SNUC_21	Normal	Good	Meta	11	CK+
	Tumor	Good	Meta	21	CD45+
	Tumor	Good	Meta	36	CK+
	Tumor	Good	Meta	37	CK+
SNUC_22	Tumor	Poor	NonMeta	29	CK+
SNUC_23	Tumor	Good	NonMeta	25	CK+
	Tumor	Good	NonMeta	26	CD45+

Figure 3. Detailed information on ROIs labeling of DSP analysis. Out of a total of 48 ROIs, there were 36 CK-positive ROIs selected to examine tumorigenesis (28 ROIs: SNUC carcinoma cells, 8 ROIs; normal epithelial cells around the tumor), and 10 ROIs were selected for CD45-positive regions to assess tumor immunity (7 ROIs: Tumor-infiltrating immune cells, 3 ROIs: immune cells in tumor-free area). We divided the groups based on the median disease-free survival of the patient cohort to determine prognosis, and we also separated the groups based on the presence of metastasis into metastasis and non-metastasis groups.

연세대학교
YONSEI UNIVERSITY

From GeoMx multiplex digital spatial profiling (DSP) analysis and then the Differentially Expressed Genes (DEG) analysis, the gene expression status of tumor cells was compared to that of normal epithelial cells. Overall features and details are summarized in Table 4 and Figure 4.

Table 4. Results of DEG analysis for gene overexpression in SNUC carcinoma cells.

Gene	Fold change	Std..Error	t.value	P-val	Significance	GSEA pathway_ count (TOP12)
H3C2	**2.854888236**	**0.648595**	**4.401651**	**0.000101**	**3.995636**	**12**
H3C7	**2.232229628**	**0.530473**	**4.207999**	**0.000178**	**3.750315**	**12**
H3C13	**2.157442542**	**0.490556**	**4.397952**	**0.000102**	**3.990929**	**12**
H3C15	**2.104124362**	**0.508755**	**4.135834**	**0.000219**	**3.659526**	**12**
H3C10	2.008093593	0.471222	4.261463	0.000152	3.817807	12
H2BC11	1.990715727	0.470389	4.232061	0.000166	3.780667	11
H2AC11	1.880055791	0.43	4.372227	0.00011	3.958214	5
H2BC9	1.87531293	0.518397	3.617522	0.000954	3.020283	11
H2AC12	1.843989603	0.453905	4.062498	0.000271	3.567655	5
H2BC10	1.839533645	0.4391	4.189327	0.000188	3.726789	11
H2AC17	1.754064515	0.450281	3.895489	0.000436	3.360055	5
H2AC21	1.638865153	0.388597	4.217393	0.000173	3.76216	5
H2BC13	1.586954299	0.282253	5.62245	2.67E-06	5.574163	11
EZH2	**1.557840722**	**0.258618**	**6.023719**	**8.02E-07**	**6.095652**	**3**

연세대학교
YONSEI UNIVERSITY

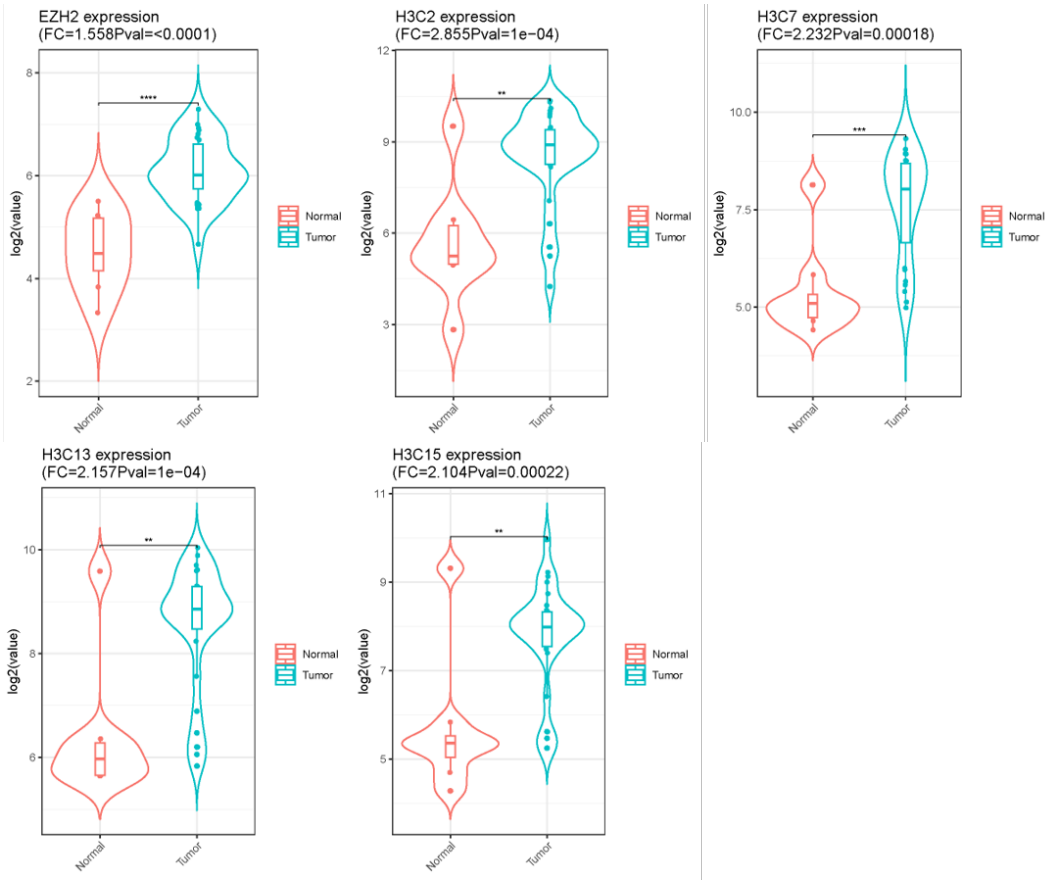

Figure 4. Wilcoxon-signed rank test images of gene expression status regarding carcinogenesis

Among several genes significantly upregulated and significantly downregulated in SNUC, the histone family gene, *H3C2* (H3 clustered histone 2) as well as *EZH2* were specifically upregulated in SNUC (fold change >1.5 times, p <0.05, Table 4, Figure 4) when compared to normal epithelial cells. In GSEA (gene set enrichment analysis), activated pathways were noted in HDAC (histone deacetylase) signaling pathway, HAT (histone

연세대학교
YONSEI UNIVERSITY

acetyltransferase) pathway, and PRC2 (polycomb repressive complex 2) pathway (Figure 5).

For downregulated genes and pathways in SNUC, downregulation of mucin family of proteins genes (*MUC5B, MUC4, MUC1, MUC5AC*), and keratin protein gene (KRT7) was noted (fold change < -1.5times, p <0.05) as well as mucin glycosylation pathway (Table 5 and Figure 5).

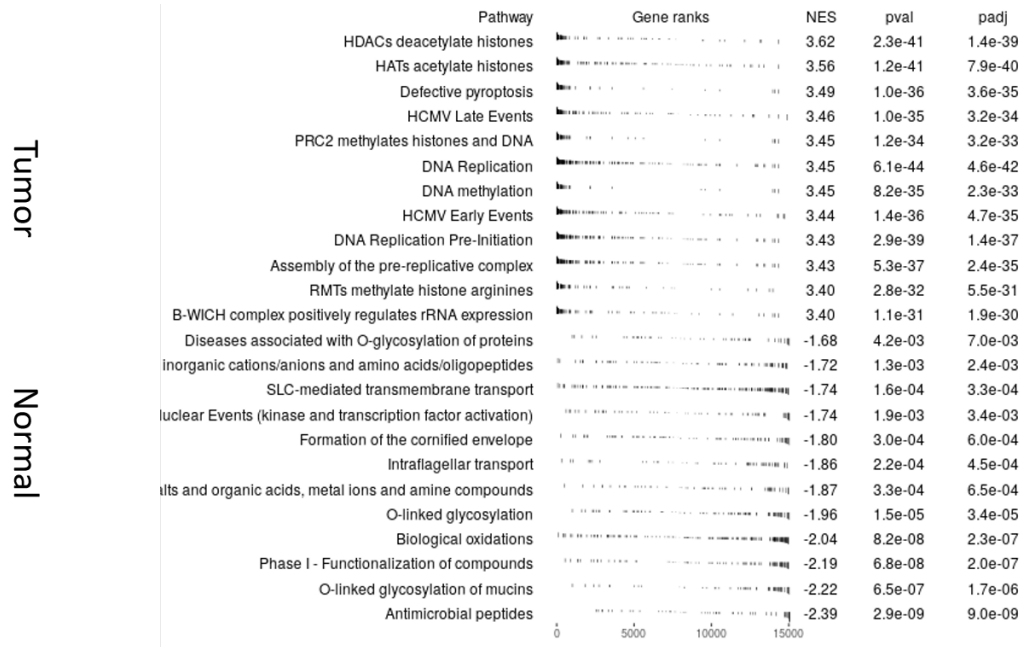

Figure 5. In GSEA (gene set enrichment analysis) image, compared with tumor and normal epithelial cells.

연세대학교
YONSEI UNIVERSITY

Table 5. Results of DEG analysis for genes downregulated in SNUC carcinoma cells.

Gene	Fold change	Std..Error	t.value	Pval	Significance	GSEA pathway_ count (TOP12)
BPIFA1	-4.89333	0.78097	-6.26572	3.90E-07	6.408961	1
BPIFB1	-4.3636	0.685944	-6.36145	2.93E-07	6.532544	1
LCN2	-3.95908	0.590786	-6.70138	1.07E-07	6.969271	1
FOS	-2.83266	0.776643	-3.64732	0.000878	3.056321	1
CLU	-2.60435	0.593541	-4.38782	0.000105	3.978042	1
MUC5B	**-2.54074**	**0.655163**	**-3.87802**	**0.000459**	**3.338485**	**3**
KRT7	**-2.50543**	**0.718719**	**-3.48596**	**0.001373**	**2.86237**	**1**
EGR1	-2.17603	0.702242	-3.09868	0.003886	2.410479	1
CP	-2.15953	0.510782	-4.22789	0.000168	3.775404	2
CYP4B1	-2.14791	0.532214	-4.0358	0.000292	3.534318	2
F3	-2.1393	0.462318	-4.62734	5.20E-05	4.284165	1
RRAD	-2.13255	0.477049	-4.4703	8.26E-05	4.083125	1
MUC4	**-2.01112**	**0.425844**	**-4.72266**	**3.92E-05**	**4.406716**	**3**
ALDH1A1	-1.83849	0.609454	-3.01661	0.004814	2.317518	2
HTN3	-1.81424	0.821127	-2.20945	0.03398	1.468776	1
SLC44A4	-1.78751	0.386299	-4.62728	5.20E-05	4.284083	2
MUC1	**-1.76002**	**0.4738**	**-3.71469**	**0.000728**	**3.138159**	**3**
CES1	-1.67024	0.45108	-3.70276	0.000752	3.123636	2
ID1	-1.66439	0.570341	-2.91824	0.006201	2.207537	1
MUC5AC	**-1.61959**	**0.481108**	**-3.36639**	**0.001903**	**2.720671**	**3**
ALDH3A1	-1.60814	0.485718	-3.31085	0.002211	2.655488	2

연세대학교
YONSEI UNIVERSITY

B. Spatial transcriptome features regarding tumor immunity

In overall, CD45-positive immune cells signals were weak in tumor area in GeoMx multiplex digital spatial profiling (DSP) analysis (such as ROI labeling 03, 10, 21, 23, 26, 40, and 47, Figure 6A). The high signal intensity of CD45-positive immune cells was mostly noted in tumor-free normal tissue areas (such as ROI labeling 14, 17, and 35, Figure 6B). When matching with H&E-stained microscopic features, tumor areas of SNUC revealed generally sparse immune cell infiltration.

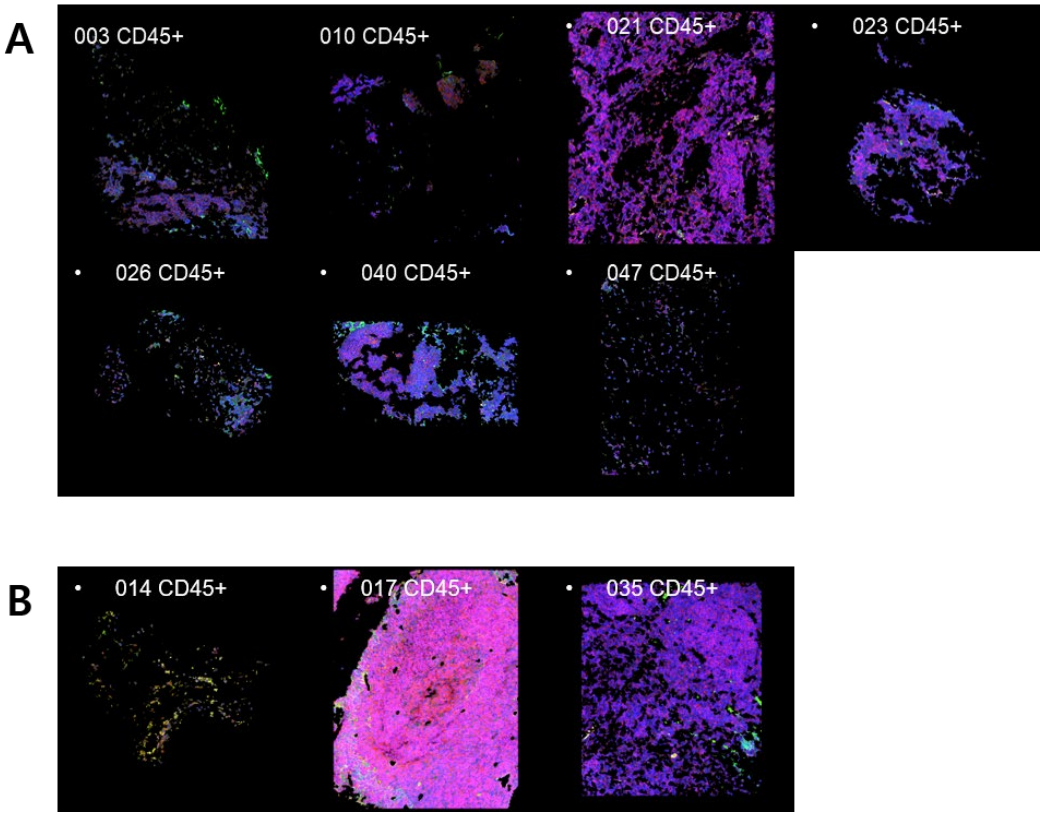

Figure 6. Immunofluorescence images of CD45 positive immune cells in intratumoral ROIs (A) and tumor-free area ROIs (B).

연세대학교
YONSEI UNIVERSITY

When comparing tumor-infiltrating immune cells to those of tumor-free normal tissue areas, only a few genes were significantly upregulated or downregulated (p-value <0.05 and fold change >1.5 or <-1.5). Although *LTF* and *TUBA3D* were noted as significantly downregulated genes, the role of these gene has not been well-known in cancers. Individual analysis of genes related to the TIME revealed no significant changes in the expression, except for the relative overexpression of LAG3 in tumor-infiltrating immune cells and a relative decreased expression of IL21 (Figure 7).

In estimated immune and stromal cell profile using SpatialDecon library with SafeTME matrix, displaying the fold change of immune cell profiles (Figure 8), an increase in the signatures of naïve B cell, macrophage, CD8 memory T cell, and Tregs was frequently noted across all 48 ROIs.

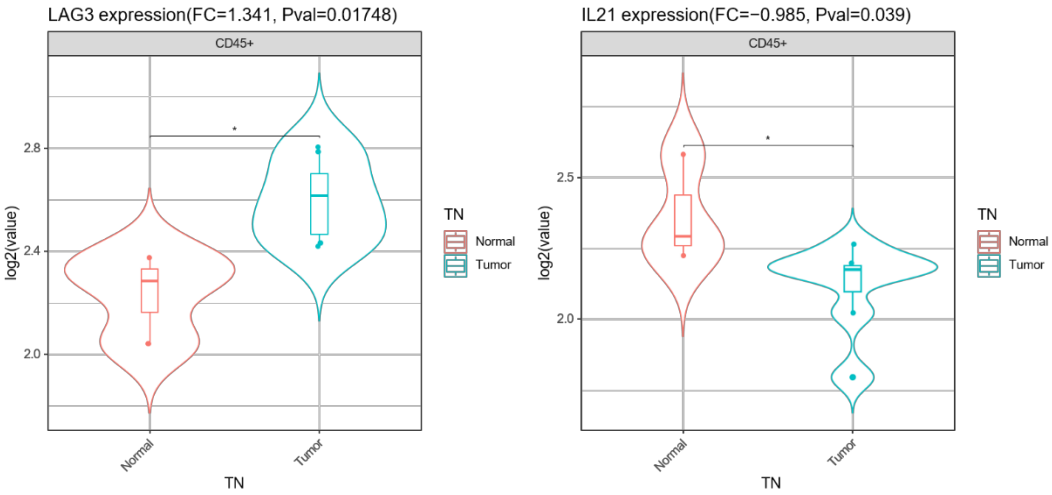

Figure 7. Wilcoxon-signed rank test images of gene expression status regarding tumor immunity.

연세대학교
YONSEI UNIVERSITY

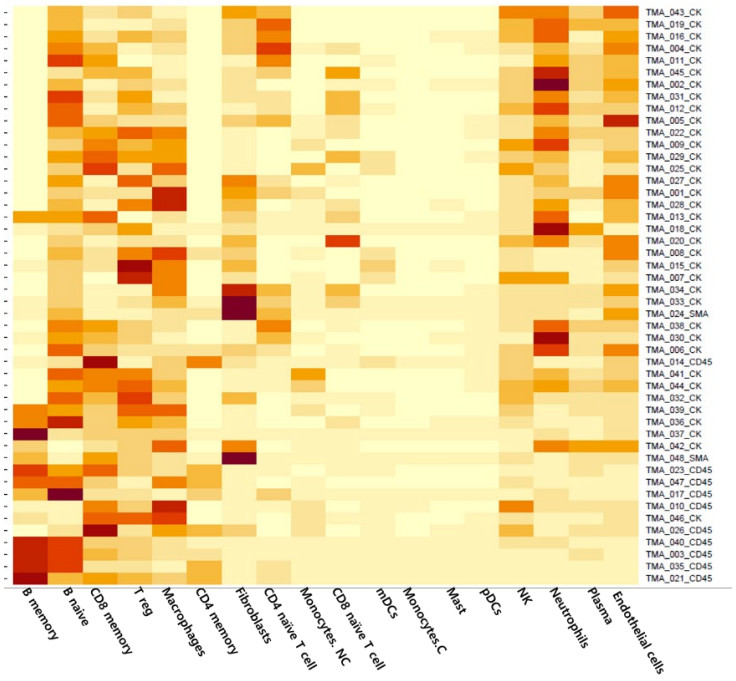

Figure 8. Estimated immune and stromal cell profile using SpatialDecon library SafeTME matrix in all 48 ROIs.

연세대학교
YONSEI UNIVERSITY

4. Investigating for genetic alterations

To identify the underlying causes for the activation of chromatin remodeling and histone modification pathways, Next-Generation Sequencing (NGS) test was performed to detect any relevant genetic alteration. The NGS study was conducted in 8 cases. The remaining 15 cases could not undergo NGS testing due to quality control (QC) failure, while 8 cases that passed the QC test were successfully tested. All 8 cases were found to be tumor mutation burden (TMB)-low, and they also showed no microsatellite instability (MSI) status. No mutation associated with the histone modification pathway of HDACs (histone deacetylases) and HAT (histone acetyltransferases), or Polycomb Repressive Complex 2 (PRC2) chromatin remodeling pathway (EZH2, SUZ12, EED) were observed. Alterations in the BMI1 gene, which is included in the PRC 1, could not be confirmed as it was not included in the NGS panel. Among 8 cases, mutations of IDH2 R172S, SMO, PTPN11, CTNNB1, ARID1A, and PMS1 genes were noted as Variants of Clinical Significance (VCS) in 4 cases. Details of detected VCS are summarized in Figure 9.

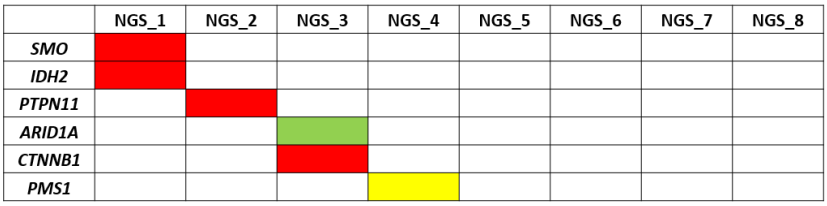

Case	Gene	Consequence	AA Change	VAF	HGVSc	HGVSp
NGS_1	*SMO*	Missense mutation	p.K575M	50	NM_005631.4:c.1724A>T	NP_005622.1:p.Lys575Met
NGS_1	*IDH2*	Missense mutation	p.R172S	10.34	NM_002168.2:c.516G>C	NP_002159.2:p.Arg172Ser
NGS_2	*PTPN11*	Missense mutation	p.T507K	17.11	NM_002834.3:c.1520C>A	NP_002825.3:p.Thr507Lys
NGS_3	*ARID1A*	Nonsense mutation	p.Q479*	25.4	NM_006015.4:c.1435C>T	NP_006006.3:p.Gln479Ter
NGS_3	*CTNNB1*	Missense mutation	p.S37A	16.56	NM_001904.3:c.109T>G	NP_001895.1:p.Ser37Ala
NGS_4	*PMS1*	Frameshift mutation	p.T216Lfs*4	40.4	NM_000534.4:c.645del	NP_000525.1:p.Thr216LeufsTer4

Figure 9. Detailed VCS information for the 8 cases. Missense mutations are marked in red, nonsense mutations in green, and frameshift mutations in yellow.

연세대학교
YONSEI UNIVERSITY

5. In vitro validation analysis

A. In vitro validation analysis of gene expression

We validated above results through in vitro study using five cell lines. FaDu, SNU1066, SNU1076, and YD10B cell lines were used as differentiated squamous cell carcinoma of head and neck, and CCL30 cell line was used as undifferentiated carcinoma of head and neck. We quantified mRNA expression of PRC2-related genes, *EZH2, EED, SUZ12*, and PRC1-related genes, *BMI1* (Figure 10A). In CCL30, the expression of *EZH2* was the highest among five cell lines and the difference was statistically significant. The expression of *EED* and *SUZ12* in CCL30 was also the highest among five cells with statistically significance. Increase of *BMI1* was not noted in CCL30 (Figure 10A). These findings indicate that CCL30, undifferentiated head and neck carcinoma, exhibited activation of PRC2 rather than PRC1. In other cell lines of FaDu, SNU1076, and SNU1066, increased expression of *EZH2, SUZ12, EED*, and *BMI1* was also observed. However, multiple relevant expressions, as observed in CCL30, were not found in these differentiated squamous cell carcinomas of the head and neck (Figure 10A). Furthermore, we examined the mRNA expression of squamous differentiation-related genes *p63, p40, KRT5 (CK5)* and *KRT6 (CK6)* (Figure 10B). Interestingly, these genes exhibited contrasting results compared to the previously mentioned PRC-2 -related complex genes. In the CCL30 cell line, the expression of p40 was significantly low, and the expression of CK5 and CK6 were also observed to be significantly low (Figure 10B), being compatible with the undifferentiated carcinoma characteristics. In case of SNU1076, significantly low expression of p63, p40, KRT5, and KRT6 was noted (Figure 10B). The moderately increased expression of EZH2 and SUZ12 may be related to the downregulation of squamous differentiation-related genes in SNU1076. This suggests that

연세대학교
YONSEI UNIVERSITY

SNU1076 may be a poorly differentiated squamous cell carcinoma. Conversely, the YD10B cell lines consistently showed no increase in PRC2 and PRC1 related genes and consistently exhibited higher expression of squamous differentiation-related genes (Figure 10B). This suggests that the YD10B cell line may be a well-differentiated squamous cell carcinoma.

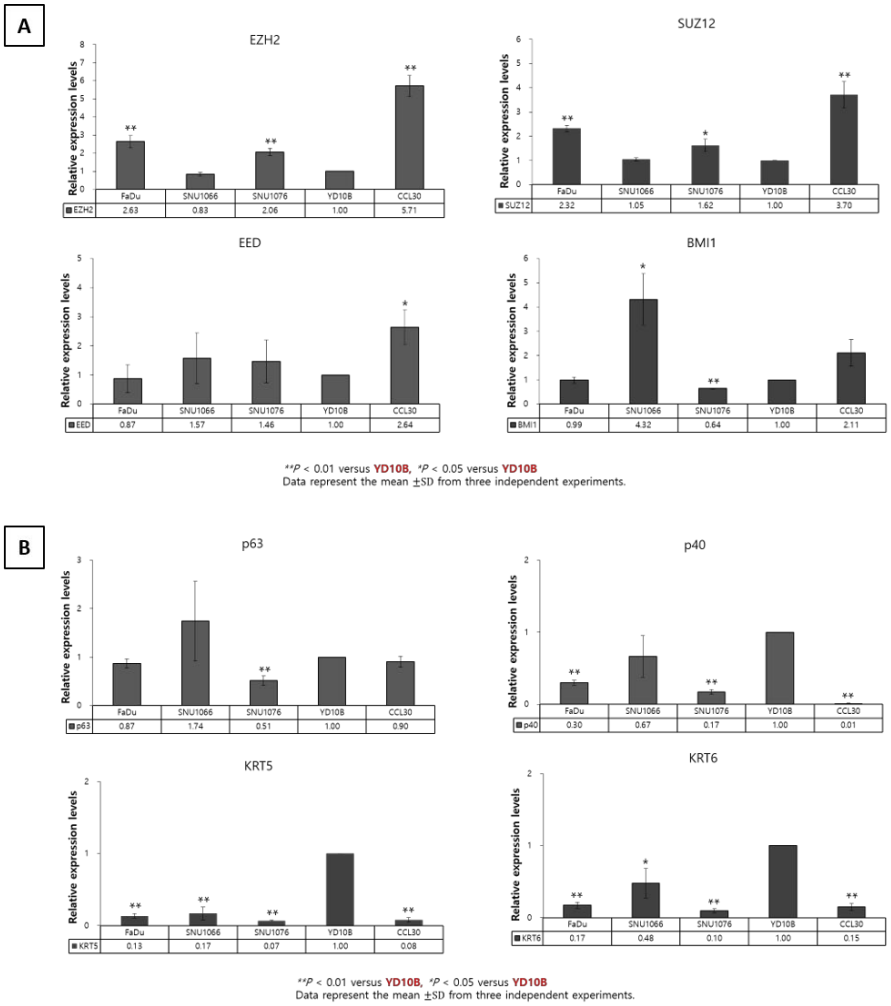

Figure 10. mRNA expression levels of PRC1/2 related genes (A) and squamous differentiated related genes (B).

연세대학교
YONSEI UNIVERSITY

B. In vitro validation analysis of protein expression

When examining protein levels through Western blot analysis, the results generally correlated with the mRNA gene expression, mentioned earlier. The CCL30 cell line exhibited relatively high expression of EZH2 and SUZ12 proteins, along with moderate expression of EED protein. In contrast, p63 and KRT 5/6 (mixture) protein expression in CCL30 was found to be extremely low (Figure 11), indicating undifferentiated carcinoma characteristics. In the case of SNU1076, this cell line exhibited relatively high expression of EZH2 and EED proteins, along with relatively low/weak expression of p63 and KRT 5/6 (mixture) proteins (Figure 11). These observations suggest characteristics of poorly differentiated squamous cell carcinoma. Conversely, YD10B cell line showed low expression of EZH2, SUZ12, and EED proteins, while displaying high expression of p63 and KRT 5/6 (mixture) proteins, indicating properties of well-differentiated squamous cell carcinoma. Furthermore, in other cell lines, we consistently observed a correlation between mRNA and protein level results, confirming the consistency of these findings.

연세대학교
YONSEI UNIVERSITY

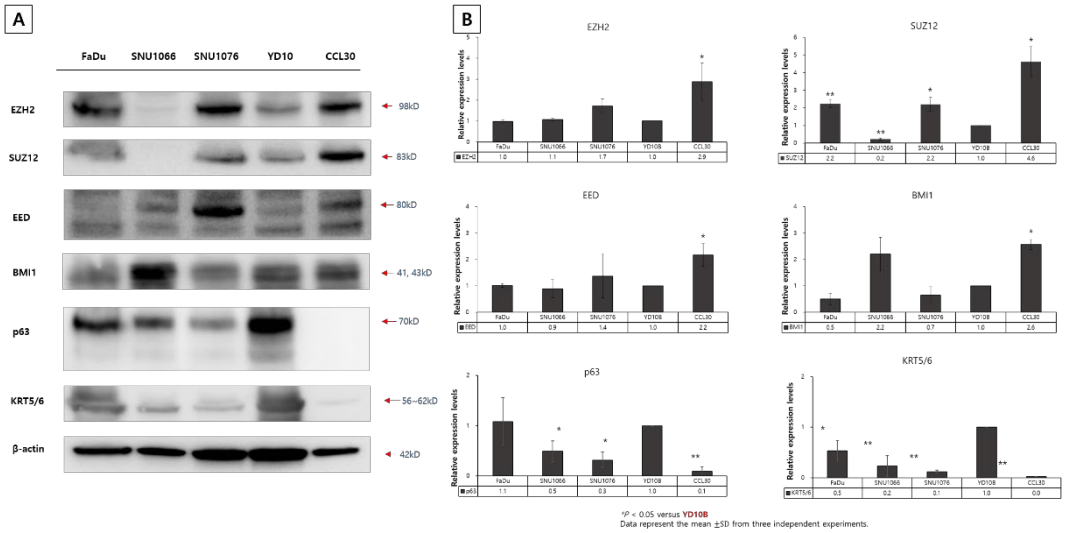

Figure11. Western blot analysis image (A) and statistical analysis (B) about PRC1/2-related proteins and squamous differentiation-related proteins.

C. In vitro validation analysis of cell morphology

We evaluated the microscopic features of the five cell lines on culture dishes and liquid-based cytology preparation (LBP) slides after harvesting and staining with Papani-colau (PAP). CCL30 showed as small round cells with scant cytoplasm and less cohesiveness, compatible with the undifferentiated tumor cell morphology. In the case of SNU1076 cell line, the cells also displayed relatively small cell size and fewer cytoplasmic processes, compared to YD10B cells. However, these cells retained cohesiveness and intercellular connections indicating a morphology consistent with poorly differentiated carcinoma. On the other hand, YD10B cells exhibited well-developed cytoplasmic processes, intercellular connections, a large cellular size, and plumb cytoplasm, indicating features consistent with well-differentiated squamous cell carcinoma. Regarding SNU1066 cells, they retained features consistent with differentiated carcinoma cells. As for FaDu cells, they appeared as large, polygonal cells with plump cytoplasm. Despite

연세대학교
YONSEI UNIVERSITY

the relatively low but retained expression of p63, KRT5, and KRT6, along with a moderate increase of EZH2, these characteristics suggest that FaDu cells may represent a large cell type of squamous cell carcinoma within the progression spectrum towards poorly differentiated or undifferentiated carcinoma. Additional visual details are listed in figure 12.

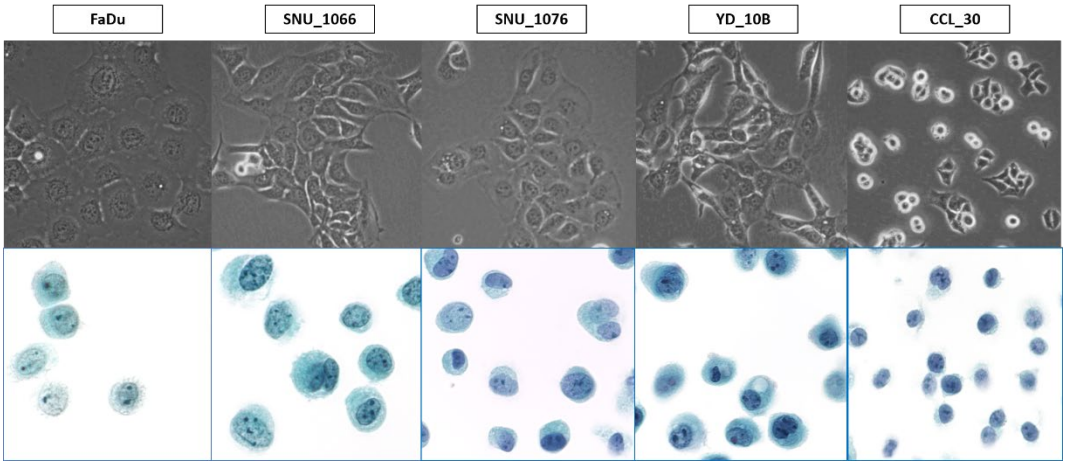

Figure 12. Microscopic features of the five cell lines. The top row shows images taken at 20x magnification on culture dish, while the bottom row shows images taken at 400x magnification after harvesting cells and staining with Papani-colau (PAP) method on liquid-based cytology preparation (LBP) slides. During the process of LBP, cells are usually dissociated into single cells, stressed, and disturbed; however, detailed cellular morphology could be additively examined under the light microscopy.

6. Validation analysis of PRC activation in clinical samples

In clinical tissue samples of SNUC, immunohistochemical expression was evaluated for EZH2, SUZ12, EED, BMI1, and H3K27me3. Expression status of representative images are presented in Figure 13. EZH2 was highly expressed in most cases with the median value 210 by H-score (160 to 300). Generally increased expression was also noted for EED (200, 30 to 300),

연세대학교
YONSEI UNIVERSITY

BMI1 (200, 50 to 300), and SUZ12 (160, 40 to 300). H3K27me3 expression (90, 30 to 300) was found to be relatively lower when compared to other PRC1/2 complexes. The increased expression of PRC2 and PRC1 complexes, as confirmed through mRNA and Western blot analyses, was consistent with the results obtained from immunohistochemistry conducted on the paraffin-embedded formalin-fixed tissue.

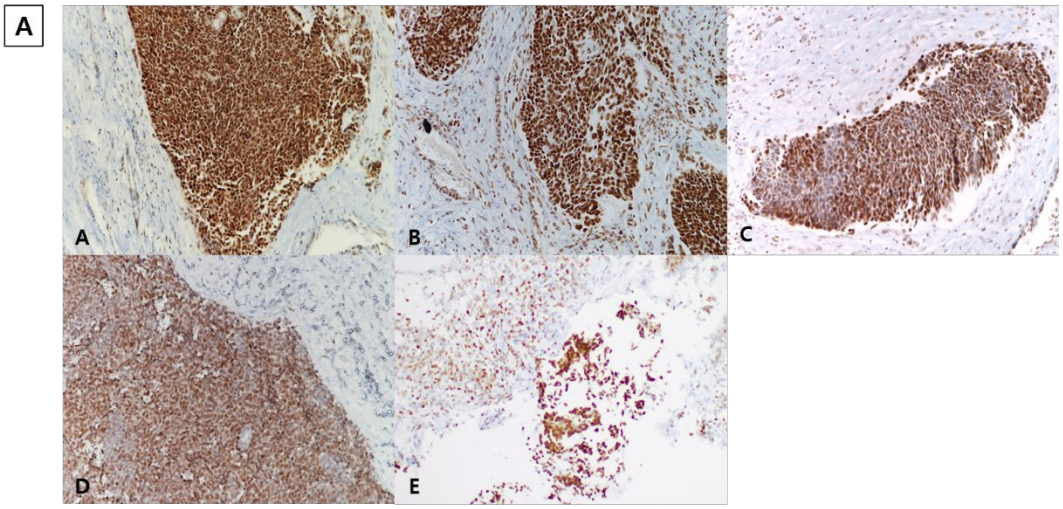

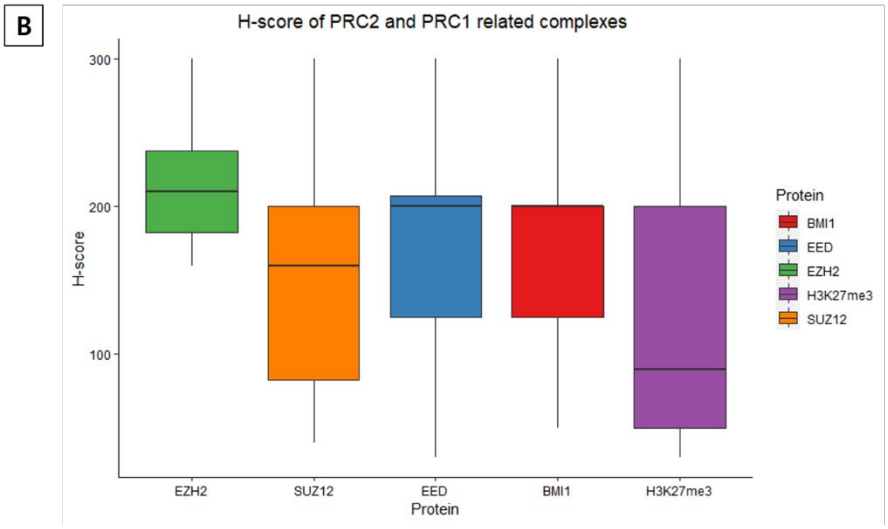

연세대학교
YONSEI UNIVERSITY

Figure 13A. Representative immunohistochemical stain image of PRC1/2 related expression. EZH2 (A), BMI1 (B), EED (C), SUZ12 (D), and H3K27me3 (E).
Figure 13B. Boxplot image of H-score results about PRC1/2 related complexes expression.

연세대학교
YONSEI UNIVERSITY

IV. DISCUSSION

This study was aimed to determine the molecular characteristics of SNUC, an extremely aggressive tumor, from the perspectives of tumorigenesis and tumor immunity. The clinical and pathological features of our SNUC cohort also exhibited aggressive carcinoma characteristics, with more than half of the cases showing advanced tumor stage at the time of diagnosis and frequent distant metastasis.

The spatial transcriptome analysis offers a notable advantage by improving the purity of the cells under study compared to conventional bulk sequencing methods. Traditional bulk sequencing struggles with the mixture of various cell types, not easy to making the isolation of specific cells of interest. In contrast, the recent spatial transcriptome analysis allowed us to precisely categorize and scrutinize four distinct cell types: tumor cells, normal epithelial cells, tumor-infiltrating immune cells, and immune cells in tumor-free areas. This capability facilitated a more comprehensive and detailed investigation. (Figure 14)

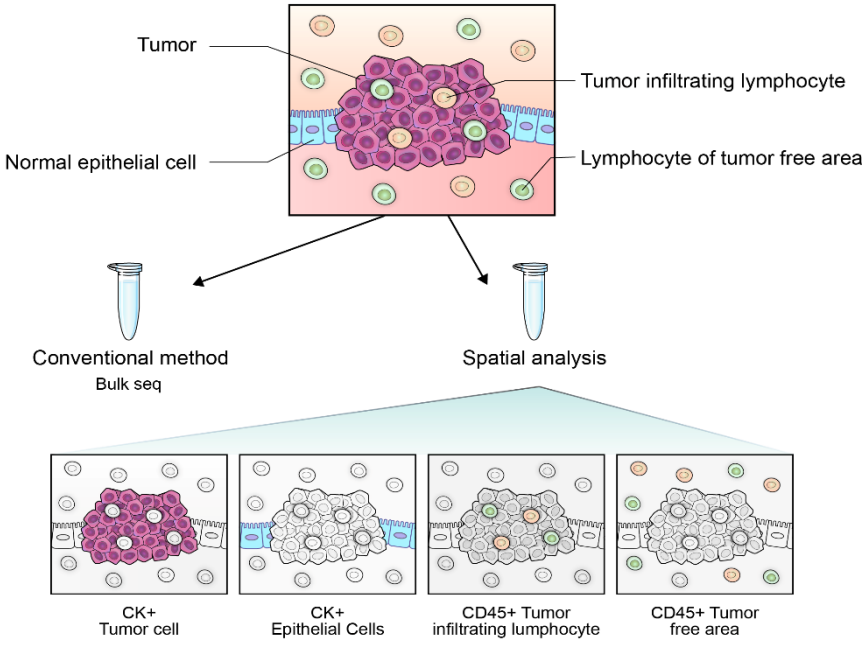

Figure 14. A schematic diagram illustrating the advantages of spatial transcriptome

연세대학교
YONSEI UNIVERSITY

analysis

In the spatial transcriptome analyses, we observed activated pathways in the PRC2 (polycomb repressive complex 2) pathway, the HDAC (Histone deacetylase) signaling pathway, and the HAT (Histone acetyltransferase) pathway including upregulation of EZH2 and histone proteins like H3C2 (H3 clustered histone 2). These results suggest that chromatin remodeling and histone modification pathways may be the dominant modes in SNUC carcinogenesis. For the downregulated genes and pathways in SNUC, we observed a decrease in mucin proteins (MUC5B, MUC4, MUC1, and MUC5AC), and the keratin protein (KRT7), as well as a reduction in the mucin glycosylation pathway. These findings might indicate the alteration of the typical cellular characteristics of normal mucosal epithelium in the sinonasal tract as the tumor progresses into undifferentiated carcinoma[19-21].

In NGS (next-generation sequencing) analyses in order to identify the underlying causes for the activation of chromatin remodeling and histone modification pathways, we could not detect genetic mutations associated with the histone modification pathway of HDACs (histone deacetylases) and HAT (histone acetyltransferases), or PRC chromatin remodeling pathway (EZH2, SUZ12, EED of PRC2). Our NGS results in SNUC suggest that activation of chromatin remodeling and histone modification pathways may occur through other signaling rather than genetic alterations. In fact, actionable/druggable gene mutations in EZH2, SUZ12, or EED are mostly observed in hematologic malignancies, and actionable mutations of HDAC or HAT have not been well elucidated yet in both solid and non-solid cancers [22-24]. Due to a lack of tissues, however, the NGS study was performed only in eight of 23 cases. There is a limitation in our study to conclude any possible roles of genetic mutation to induce chromatin remodeling and histone modification pathway alteration in our study, thus, further study should be followed with more tissue samples.

연세대학교
YONSEI UNIVERSITY

Interestingly, we noted mutations of *IDH2 R172S, SMO, PTPN11, CTNNB1, ARID1A*, and *PMS1* genes as variants of clinical significance (VCS) in 4 cases. *IDH2* hotspot mutations are recently known in SNUC with the frequency of 33-85% with *IDH2 R172S* mutation being the most common [4, 5, 25, 26].

The *IDH* gene plays a crucial role in the Krebs cycle and in maintaining cellular homeostasis [27]. *IDH* mutation is well known as alleged roles to induce DNA hypermethylation in several types of malignancies such as glioma [28, 29], acute myeloid leukemia [30, 31], chondrosarcoma [32], cholangiocarcinoma [33], and angioimmunoblastic T cell lymphoma [34]. SNUC with *IDH2* mutation is known to show hypermethylation phenotype, and studies based on DNA methylation profiling indicate that *IDH*-mutant sinonasal malignancies form a separate category from tumor types without *IDH* mutation [6].

SWI/SNF complex-deficient sinonasal carcinoma is a recently defined entity by WHO classification [1]. Analogous to SNUC, this tumor is defined as a poorly differentiated to undifferentiated carcinoma that exhibits the loss of one SWI/SNF complex subunit (SMARCB1/INI1 or SMARCA4/BRG1) without histologic differentiation, leading to its classification as a specific entity. The SWI/SNF complex genes are also known to be related to chromatin remodeling [35-37].

Regarding the epigenetic roles of DNA methylation [6], chromatin remodeling-related SWI/SNF alteration [8], and considering our findings of activated chromatin remodeling and histone modification pathways as well as rarity of genetic alteration, SNUC and its analogies of undifferentiated carcinoma arising in sinonasal tracts seem to mainly use epigenetic methods in carcinogenesis.

Other altered genes in our study may also play a role in carcinogenesis of SNUC regarding their well-known roles as oncogenes or tumor suppressor genes: a gain-of-function mutation in the *SMO* gene, implicated in the Sonic hedgehog pathway; a gain-of-function mutation in the *PTPN11* gene, involved in the PIK3K/AKT and RAS signaling pathways; a gain-of-function mutation in the *CTNNB1* gene, associated with the WNT signaling pathway; a truncating mutation in the tumor suppressor gene *ARID1A,* linked to

연세대학교
YONSEI UNIVERSITY

the SWI/SNF chromatin-remodeling complex; and lastly, a truncating mutation in the *PMS1* gene, a participant in DNA mismatch repair.

In vitro validation analyses of undifferentiated and poorly differentiated carcinoma cell lines of the head and neck showed overexpression of EZH2 and related PRC2-related molecules (SUZ12 and EED) at the mRNA and protein levels. Furthermore, the activation of PRC-related molecules was related to the contrasting downregulation of squamous cell differentiation-related molecules, such as p63, p40, KRT5, and KRT6. Integrating the results of RNA gene and protein expression, reveals an inverse relationship between PRC-related molecules and differentiation-related molecules, along with the cell line morphology of undifferentiated/poorly differentiated/well-differentiated type. This suggests that PRC-related chromatin remodeling pathway may play a crucial role in the progression of tumors into undifferentiated carcinoma. Clinical tissues of SNUC also generally demonstrated high immunoexpression of PRC-related proteins including EZH2 and supported the above results of spatial transcriptome profiles and in vitro analyses.

Considering the spatial transcriptome profiles of SNUC tumor tissues, it appears that EZH2 may take a leading role in the activation of the PRC-related chromatin remodeling process, since other PRC-related genes such as SUZ12, EED, and BMI1 were not upregulated in SNUC tumor tissue. Regarding histone modification, it may either follow EZH2-led PRC activation or occur in parallel. Notably, our spatial transcriptome analysis data did not show direct activation of HDAC or HAT. Therefore, it is plausible that EZH2 serves as an initiating factor, leading to subsequent signaling in chromatin remodeling and histone modification during the development of SNUC.

Epigenetic modifications have the capacity to control the state of chromatin and gene expression by means of processes such as DNA methylation and demethylation, histone modification, chromatin remodeling, and more, all without modifying the underlying DNA sequences[38, 39]. Polycomb group proteins (PcGs), a crucial set of epigenetic regulators, have a considerable role in regulating cell proliferation and are essential factors in maintaining pluripotency and guiding the differentiation of stem cells. Additionally,

연세대학교
YONSEI UNIVERSITY

they are implicated in the abnormal gene expression patterns observed during the development of malignancies [38]. EZH2, a gene conserved across different species throughout evolution, displays analogous structural patterns and functional domains. Acting as a histone methyltransferase, EZH2 acts as the catalytic component within PRC2, tasked with the tri-methylation of histone H3 at Lys 27 (H3K27me3). This methylation process results in gene silencing, affecting a wide range of biological functions, including cell cycle regulation, proliferation, and differentiation [40]. The importance of EZH2 in cancer progression has been highlighted, as its increased expression has been observed in various malignancies.

EZH2 plays an oncogenic role in various cancers, both solid tumors (such as breast cancer [41], prostate cancer [42], esophageal cancer [43], gastric cancer [44], anaplastic thyroid carcinoma [45], and endometrial carcinoma [46]) and hematologic malignancies [47] (such as follicular lymphoma [48]). In malignant tumor models, EZH2 plays a crucial role in promoting tumor growth and metastasis by mediating H3K27me3 [49, 50]. As stated previously, given the numerous significant functions of EZH2 in cancer, therapeutic approaches directed at targeting EZH2 have emerged as vital strategies in the treatment of various cancer types [50, 51].

The observed relationship between EZH2 and SNUC tumorigenesis suggests that EZH2 plays a significant role in SNUC development and may be a potential candidate for EZH2-targeted therapy. In addition, combining our study results and previously known characteristics for undifferentiated carcinoma arising in sinonasal tract, we suggest that EZH2-activated SNUC is a molecular subset of SNUC and its analogies. (Figure 14)

Considering the relatively immune-poor microenvironment observed in the histology of SNUC and the current spatial transcriptome results, it appears that tumor immunity may not play a pivotal role in the development of SNUC. Alternatively, it's possible that a relatively immune-poor microenvironment forms as a mechanism of immune escape in this aggressive tumor after it has developed into SNUC. It has become that the expression of EZH2 in cancer cells suppresses tumor immunity. In ovarian tumors, EZH2 expression

연세대학교
YONSEI UNIVERSITY

hinders the production of CXCL9, which is vital for the infiltration of CD8+ T cells [52, 53]. In the context of glioblastoma, the inhibition of EZH2 using siEZH2 leads to a reduction in the expression of M2 markers, indicating the significant role of EZH2 in pushing microglia towards M2 phenotype. M2-type tumor-associated macrophages contribute to diminishing the anti-tumor response and promoting tumor growth through the release of various cytokines [54]. To investigate any possible role of EZH2 in forming immune-poor microenvironment of SNUC, additional studies using animal models capable of observing the time-series development of tumors may be warranted.

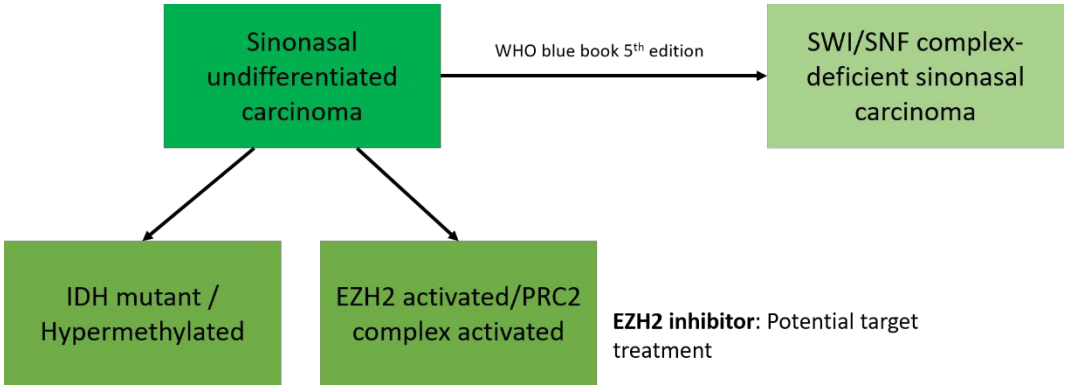

Figure 15. Presentation of a new molecular subset of SNUC.

연세대학교
YONSEI UNIVERSITY

V. CONCLUSION

SNUC presents a challenge in oncology because of its rare occurrence, aggressive behavior, and limited treatment options. In this study, we tried to clarify the molecular characteristics of SNUC, with a focus on tumorigenesis and tumor immunity.

Our study suggests that SNUC mainly uses epigenetic modes in tumorigenesis through chromatin remodeling rather than genetic alteration. EZH2 activation was observed in SNUC tumor cells and suggested EZH2 being crucial in carcinogenesis of SNUC. Thus, targeting EZH2 using inhibitors may offer a potential avenue for improving treatment outcomes. This study had limitations, and further research is needed to fully explore the regulatory mechanisms underlying EZH2 activation and its therapeutic implications.

연세대학교
YONSEI UNIVERSITY

REFERENCES

1. Bishop JA, Thompson LDR, Loney EL, et al. WHO Classification of Tumours Editorial Board. Head and neck tumours [Internet; beta version ahead of print]. International Agency for Research on Cancer; 2022 [cited 2023 09 01]. (WHO classification of tumours series, 5th ed.; vol. 9). Accessed September 1, 2022.
2. Chambers KJ, Lehmann AE, Remenschneider A, et al. Incidence and survival patterns of sinonasal undifferentiated carcinoma in the United States. *J Neurol Surg B Skull Base*. Mar 2015;76(2):94-100. doi:10.1055/s-0034-1390016
3. Frierson HF, Jr., Mills SE, Fechner RE, Taxy JB, Levine PA. Sinonasal undifferentiated carcinoma. An aggressive neoplasm derived from schneiderian epithelium and distinct from olfactory neuroblastoma. *Am J Surg Pathol*. Nov 1986;10(11):771-9.
4. Dogan S, Chute DJ, Xu B, et al. Frequent IDH2 R172 mutations in undifferentiated and poorly-differentiated sinonasal carcinomas. *J Pathol*. Aug 2017;242(4):400-408. doi:10.1002/path.4915
5. Jo VY, Chau NG, Hornick JL, Krane JF, Sholl LM. Recurrent IDH2 R172X mutations in sinonasal undifferentiated carcinoma. *Mod Pathol*. May 2017;30(5):650-659. doi:10.1038/modpathol.2016.239
6. Dogan S, Vasudevaraja V, Xu B, et al. DNA methylation-based classification of sinonasal undifferentiated carcinoma. *Mod Pathol*. Oct 2019;32(10):1447-1459. doi:10.1038/s41379-019-0285-x
7. Chowdhury R, Yeoh KK, Tian YM, et al. The oncometabolite 2-hydroxyglutarate inhibits histone lysine demethylases. *EMBO Rep*. May 2011;12(5):463-9. doi:10.1038/embor.2011.43
8. Heft Neal ME, Birkeland AC, Bhangale AD, et al. Genetic analysis of sinonasal undifferentiated carcinoma discovers recurrent SWI/SNF alterations and a novel PGAP3-SRPK1 fusion gene. *BMC Cancer*. May 29 2021;21(1):636.

연세대학교
YONSEI UNIVERSITY

doi:10.1186/s12885-021-08370-x

9. Wilson BG, Roberts CW. SWI/SNF nucleosome remodellers and cancer. *Nat Rev Cancer*. Jun 9 2011;11(7):481-92. doi:10.1038/nrc3068
10. Denaro N, Merlano M, Numico G, Garrone O, Bossi P. Complete response to immunotherapy in sinonasal undifferentiated carcinoma. *Tumori*. Dec 2021;107(6):Np101-np104. doi:10.1177/03008916211026971
11. Villanueva-Fernández E, Hermsen MA, Suárez-Fernández L, et al. Biomarkers for Immunotherapy in Poorly Differentiated Sinonasal Tumors. *Biomedicines*. Sep 6 2022;10(9)doi:10.3390/biomedicines10092205
12. de Visser KE, Joyce JA. The evolving tumor microenvironment: From cancer initiation to metastatic outgrowth. *Cancer Cell*. Mar 13 2023;41(3):374-403. doi:10.1016/j.ccell.2023.02.016
13. Binnewies M, Roberts EW, Kersten K, et al. Understanding the tumor immune microenvironment (TIME) for effective therapy. *Nat Med*. May 2018;24(5):541-550. doi:10.1038/s41591-018-0014-x
14. Enepekides DJ. Sinonasal undifferentiated carcinoma: an update. *Curr Opin Otolaryngol Head Neck Surg*. Aug 2005;13(4):222-5. doi:10.1097/01.moo.0000172806.56382.eb
15. Musy PY, Reibel JF, Levine PA. Sinonasal undifferentiated carcinoma: the search for a better outcome. *Laryngoscope*. Aug 2002;112(8 Pt 1):1450-5. doi:10.1097/00005537-200208000-00023
16. Robinson KM, Hawkins AS, Santana-Cruz I, et al. Aligner optimization increases accuracy and decreases compute times in multi-species sequence data. *Microb Genom*. Sep 2017;3(9):e000122. doi:10.1099/mgen.0.000122
17. Cibulskis K, Lawrence MS, Carter SL, et al. Sensitive detection of somatic point mutations in impure and heterogeneous cancer samples. *Nat Biotechnol*. Mar 2013;31(3):213-9. doi:10.1038/nbt.2514
18. Danaher P, Kim Y, Nelson B, et al. Advances in mixed cell deconvolution enable

연세대학교
YONSEI UNIVERSITY

quantification of cell types in spatial transcriptomic data. *Nat Commun*. Jan 19 2022;13(1):385. doi:10.1038/s41467-022-28020-5

19. Truong AB, Kretz M, Ridky TW, Kimmel R, Khavari PA. p63 regulates proliferation and differentiation of developmentally mature keratinocytes. *Genes Dev*. Nov 15 2006;20(22):3185-97. doi:10.1101/gad.1463206
20. Stefansson IM, Salvesen HB, Akslen LA. Loss of p63 and cytokeratin 5/6 expression is associated with more aggressive tumors in endometrial carcinoma patients. *Int J Cancer*. Mar 1 2006;118(5):1227-33. doi:10.1002/ijc.21415
21. Reis-Filho JS, Simpson PT, Martins A, Preto A, Gärtner F, Schmitt FC. Distribution of p63, cytokeratins 5/6 and cytokeratin 14 in 51 normal and 400 neoplastic human tissue samples using TARP-4 multi-tumor tissue microarray. *Virchows Arch*. Aug 2003;443(2):122-32. doi:10.1007/s00428-003-0859-2
22. Chakravarty D, Gao J, Phillips SM, et al. OncoKB: A Precision Oncology Knowledge Base. *JCO Precis Oncol*. Jul 2017;2017doi:10.1200/po.17.00011
23. Lue JK, Amengual JE. Emerging EZH2 Inhibitors and Their Application in Lymphoma. *Curr Hematol Malig Rep*. Oct 2018;13(5):369-382. doi:10.1007/s11899-018-0466-6
24. Lee HZ, Kwitkowski VE, Del Valle PL, et al. FDA Approval: Belinostat for the Treatment of Patients with Relapsed or Refractory Peripheral T-cell Lymphoma. *Clin Cancer Res*. Jun 15 2015;21(12):2666-70. doi:10.1158/1078-0432.Ccr-14-3119
25. Mito JK, Bishop JA, Sadow PM, et al. Immunohistochemical Detection and Molecular Characterization of IDH-mutant Sinonasal Undifferentiated Carcinomas. *Am J Surg Pathol*. Aug 2018;42(8):1067-1075. doi:10.1097/pas.0000000000001064
26. Riobello C, López-Hernández A, Cabal VN, et al. IDH2 Mutation Analysis in Undifferentiated and Poorly Differentiated Sinonasal Carcinomas for Diagnosis and Clinical Management. *Am J Surg Pathol*. Mar 2020;44(3):396-405. doi:10.1097/pas.0000000000001420
27. Lee S, Urman A, Desai P. Emerging drug profile: Krebs cycle and cancer: IDH

연세대학교
YONSEI UNIVERSITY

mutations and therapeutic implications. *Leuk Lymphoma*. Nov 2019;60(11):2635-2645. doi:10.1080/10428194.2019.1602260

28. Han S, Liu Y, Cai SJ, et al. IDH mutation in glioma: molecular mechanisms and potential therapeutic targets. *Br J Cancer*. May 2020;122(11):1580-1589. doi:10.1038/s41416-020-0814-x
29. Yan H, Parsons DW, Jin G, et al. IDH1 and IDH2 mutations in gliomas. *N Engl J Med*. Feb 19 2009;360(8):765-73. doi:10.1056/NEJMoa0808710
30. Ley TJ, Miller C, Ding L, et al. Genomic and epigenomic landscapes of adult de novo acute myeloid leukemia. *N Engl J Med*. May 30 2013;368(22):2059-74. doi:10.1056/NEJMoa1301689
31. Marcucci G, Maharry K, Wu YZ, et al. IDH1 and IDH2 gene mutations identify novel molecular subsets within de novo cytogenetically normal acute myeloid leukemia: a Cancer and Leukemia Group B study. *J Clin Oncol*. May 10 2010;28(14):2348-55. doi:10.1200/jco.2009.27.3730
32. Amary MF, Bacsi K, Maggiani F, et al. IDH1 and IDH2 mutations are frequent events in central chondrosarcoma and central and periosteal chondromas but not in other mesenchymal tumours. *J Pathol*. Jul 2011;224(3):334-43. doi:10.1002/path.2913
33. Boscoe AN, Rolland C, Kelley RK. Frequency and prognostic significance of isocitrate dehydrogenase 1 mutations in cholangiocarcinoma: a systematic literature review. *J Gastrointest Oncol*. Aug 2019;10(4):751-765. doi:10.21037/jgo.2019.03.10
34. Wang C, McKeithan TW, Gong Q, et al. IDH2R172 mutations define a unique subgroup of patients with angioimmunoblastic T-cell lymphoma. *Blood*. Oct 8 2015;126(15):1741-52. doi:10.1182/blood-2015-05-644591
35. Mittal P, Roberts CWM. The SWI/SNF complex in cancer - biology, biomarkers and therapy. *Nat Rev Clin Oncol*. Jul 2020;17(7):435-448. doi:10.1038/s41571-020-0357-3
36. Wilson BG, Wang X, Shen X, et al. Epigenetic antagonism between polycomb and SWI/SNF complexes during oncogenic transformation. *Cancer Cell*. Oct 19

연세대학교
YONSEI UNIVERSITY

2010;18(4):316-28. doi:10.1016/j.ccr.2010.09.006

37. Januario T, Ye X, Bainer R, et al. PRC2-mediated repression of SMARCA2 predicts EZH2 inhibitor activity in SWI/SNF mutant tumors. *Proc Natl Acad Sci U S A*. Nov 14 2017;114(46):12249-12254. doi:10.1073/pnas.1703966114
38. Margueron R, Reinberg D. The Polycomb complex PRC2 and its mark in life. *Nature*. Jan 20 2011;469(7330):343-9. doi:10.1038/nature09784
39. Greer EL, Shi Y. Histone methylation: a dynamic mark in health, disease and inheritance. *Nat Rev Genet*. Apr 3 2012;13(5):343-57. doi:10.1038/nrg3173
40. Di Croce L, Helin K. Transcriptional regulation by Polycomb group proteins. *Nat Struct Mol Biol*. Oct 2013;20(10):1147-55. doi:10.1038/nsmb.2669
41. Kleer CG, Cao Q, Varambally S, et al. EZH2 is a marker of aggressive breast cancer and promotes neoplastic transformation of breast epithelial cells. *Proc Natl Acad Sci U S A*. Sep 30 2003;100(20):11606-11. doi:10.1073/pnas.1933744100
42. Xin L. EZH2 accompanies prostate cancer progression. *Nat Cell Biol*. Sep 2021;23(9):934-936. doi:10.1038/s41556-021-00744-4
43. Qiu BQ, Lin XH, Ye XD, et al. Long non-coding RNA PSMA3-AS1 promotes malignant phenotypes of esophageal cancer by modulating the miR-101/EZH2 axis as a ceRNA. *Aging (Albany NY)*. Jan 31 2020;12(2):1843-1856. doi:10.18632/aging.102716
44. Gan L, Xu M, Hua R, et al. The polycomb group protein EZH2 induces epithelial-mesenchymal transition and pluripotent phenotype of gastric cancer cells by binding to PTEN promoter. *J Hematol Oncol*. Jan 15 2018;11(1):9. doi:10.1186/s13045-017-0547-3
45. Pellecchia S, Sepe R, Decaussin-Petrucci M, et al. The Long Non-Coding RNA Prader Willi/Angelman Region RNA5 (PAR5) Is Downregulated in Anaplastic Thyroid Carcinomas Where It Acts as a Tumor Suppressor by Reducing EZH2 Activity. *Cancers (Basel)*. Jan 17 2020;12(1)doi:10.3390/cancers12010235
46. Krill L, Deng W, Eskander R, et al. Overexpression of enhance of Zeste homolog 2

연세대학교
YONSEI UNIVERSITY

(EZH2) in endometrial carcinoma: An NRG Oncology/Gynecologic Oncology Group Study. *Gynecol Oncol*. Feb 2020;156(2):423-429. doi:10.1016/j.ygyno.2019.12.003

47. Li B, Chng WJ. EZH2 abnormalities in lymphoid malignancies: underlying mechanisms and therapeutic implications. *J Hematol Oncol*. Nov 21 2019;12(1):118. doi:10.1186/s13045-019-0814-6
48. Bödör C, O'Riain C, Wrench D, et al. EZH2 Y641 mutations in follicular lymphoma. *Leukemia*. Apr 2011;25(4):726-9. doi:10.1038/leu.2010.311
49. Pasini D, Di Croce L. Emerging roles for Polycomb proteins in cancer. *Curr Opin Genet Dev*. Feb 2016;36:50-8. doi:10.1016/j.gde.2016.03.013
50. Kim KH, Roberts CW. Targeting EZH2 in cancer. *Nat Med*. Feb 2016;22(2):128-34. doi:10.1038/nm.4036
51. Duan R, Du W, Guo W. EZH2: a novel target for cancer treatment. *J Hematol Oncol*. Jul 28 2020;13(1):104. doi:10.1186/s13045-020-00937-8
52. Peng D, Kryczek I, Nagarsheth N, et al. Epigenetic silencing of TH1-type chemokines shapes tumour immunity and immunotherapy. *Nature*. Nov 12 2015;527(7577):249-53. doi:10.1038/nature15520
53. Dangaj D, Bruand M, Grimm AJ, et al. Cooperation between Constitutive and Inducible Chemokines Enables T Cell Engraftment and Immune Attack in Solid Tumors. *Cancer Cell*. Jun 10 2019;35(6):885-900.e10. doi:10.1016/j.ccell.2019.05.004
54. Yin Y, Qiu S, Li X, Huang B, Xu Y, Peng Y. EZH2 suppression in glioblastoma shifts microglia toward M1 phenotype in tumor microenvironment. *J Neuroinflammation*. Nov 13 2017;14(1):220. doi:10.1186/s12974-017-0993-4

연세대학교
YONSEI UNIVERSITY

ABSTRACT(IN KOREAN)

비강상악동 미분화암종의 분자병리적 특성 규명

<지도교수 윤 선 옥 >

연세대학교 대학원 의학과

류 향 주

비강상악동 미분화암종 (SNUC)은 비강 및 부비동에서 기원하는 드물고 매우 공격적인 암종이다. 조직학적으로 다른 편평세포, 선샘, 신경내분비세포의 분화를 배제하면 진단할 수 있다. 비강상악동 미분화암종은 좋지 않은 예후를 보이며, 그 종양이 생기는 병인과 종양면역에 대한 이해가 제한적이다.
본 연구에서는 비강상악동 미분화암종의 분자적 특성을 탐색하였으며, 특히 종양 발생 및 종양면역에 중점을 두었다. 공간 전사체 분석을 통해 활성화된 염색질 리모델링 경로 (chromatin remodeling pathway) 와 히스톤 변형 경로 (histone modification pathway) 및, 특히 EZH2 유전자의 과발현이 확인되었다. 이러한 결과를 통해 유전자 변조 메커니즘 (epigenetic mechanism) 이 비강상악동 미분화암종의 발생에 관여할 수 있음을 시사하였다.
시험관 내 분석에서, EZH2, SUZ12, 및 EED와 같은 다른 PRC2 (polycomb repressive complex-2) 관련 염색질 재구조화 표지자의 mRNA와 단백질의 농도가 미분화된 편평세포암 세포주에서 상승됨을 확인하였으며, 편평세포 분화 표지자인 p40, p63, KRT5, 및 KRT6 은 미분화된 편평세포암 세포주에서 감소함을 확인하였다. 이러한 결과는 환자에게서 얻어진 조직에서 시행한 면역조직화학염색결과에서도 유사하게 EZH2 및 다른 PRC2 표지자의 면역표현형이 증가함을 한번 더 확인하였다. 이는 미분화성 암 발행에 있어 EZH2 가 중요한 역할을 하는 것임을 시사할 수 있었다. 본 연구에서 SNUC의 발병과 종양면역의 역할에 대한 구체적인 결과는 확인되지 않았다.

연세대학교
YONSEI UNIVERSITY

EZH2 활성화에 의해 유도되는 유전자 변형은 SNUC의 병인 발생의 주요 원인으로 판단되며, EZH2는 SNUC를 포함한 다양한 암 종양에서 발견되는 변이로, 잠재적 치료 대상이 될 수 있을 것이다. 비강상악동 미분화암종에서 상대적으로 빈약한 종양 면역 미세환경에도 불구하고, 이 종양의 발병과 잠재적인 면역회피 메커니즘에 대한 연구는 추후 필요할 것으로 생각된다.
결론적으로, 본 연구를 통하여 비강상악동 미분화암종의 분자적 병인을 밝힘에 있어 EZH2가 중요한 역할을 하며 이를 타겟으로 하는 잠재적 치료 대상이 될 수 있을 것임을 제안하며 연구를 마친다.

핵심되는 말 : 비강상악동 미분화암종, EZH2, 종양 발생